

Article

# Efficient Antifungal and Flame-Retardant Properties of ZnO-TiO<sub>2</sub>-Layered Double-Nanostructures Coated on Bamboo Substrate

Danjing Ren, Jingpeng Li \* , Jun Xu, Zaixing Wu , Yongjie Bao, Neng Li and Yuhe Chen \*

Key Laboratory of High Efficient Processing of Bamboo of Zhejiang Province, China National Bamboo Research Center, Chinese Academy of Forestry, Hangzhou 310012, China; rdjing@yeah.net (D.R.); ssnhcy@hotmail.com (J.X.); jansonwu@126.com (Z.W.); baoyongjie1@126.com (Y.B.); lineng8657@sina.com (N.L)

\* Correspondence: lijip@caf.ac.cn (J.L.); yuhec@sina.com (Y.C.)

Received: 20 August 2018; Accepted: 19 September 2018; Published: 26 September 2018



**Abstract:** A facile method to synthesize ZnO-TiO<sub>2</sub>-layered double-nanostructures with the average thickness of 20 μm on a bamboo substrate was proposed to improve the antifungal and flame-retardant properties. The cross-linked wurtzite ZnO nanostructures with an average thickness of approximately 0.14 μm were uniformly distributed on the anatase TiO<sub>2</sub> surface. The energy-dispersive X-ray spectroscopy (EDS) confirmed that the ZnO-TiO<sub>2</sub> coating on bamboo was a layered double nanostructure. During a two-month antifungal test conducted in an outdoor environment, the fungi began to grow after one week on pristine bamboo and three weeks on ZnO-bamboo and TiO<sub>2</sub>-bamboo. Furthermore, there was an infected area of 100% after four weeks for pristine bamboo and six weeks for ZnO-bamboo, while there was an infected area of 43% after eight weeks for TiO<sub>2</sub>-bamboo. By comparison, there was no visible fungal growth on ZnO-TiO<sub>2</sub>-bamboo until the end of the test. The electron spin resonance (ESR) technique has demonstrated that the reactive oxygen species (ROS) of •O<sub>2</sub><sup>-</sup> and •OH were produced from the ZnO-TiO<sub>2</sub> surface under visible light irradiation (λ > 420 nm). This large quantity of •O<sub>2</sub><sup>-</sup> compared to •OH is considered to be mainly responsible for the inactivation of fungi. Additionally, the limiting oxygen index has increased from 25.6% to 30.2% after being covered with a ZnO-TiO<sub>2</sub> coating, which revealed a significant enhancement of its flame-retardant property.

**Keywords:** bamboo; TiO<sub>2</sub>; ZnO; layered double nanostructures; antifungal property; flame-retardant property

## 1. Introduction

Bamboo is an abundant natural resource in China. It has excellent physical and mechanical properties, such as low weight, easy machining, high intensity, and flexibility [1]. As a rapidly renewable sustainable resource, bamboo has been extensively applied in the production of bamboo-based composites, such as laminated bamboo board, bamboo particle board, bamboo plywood, and bamboo scrimber [2–4]. Due to its diverse usage and fast growth rate, bamboo has become an ideal material to satisfy the demands for wood. Bamboo is increasingly being utilized worldwide as an essential raw material for construction industry [5]. However, bamboo is easily infected with fungi because of its hygroscopicity and organic nature. With the increasing application of bamboo in an outdoor environment, it is necessary to develop an effective antifungal technique to protect bamboo in a natural environment. Meanwhile, the flammability of bamboo also restricts its utilization, with fire safety being a major concern for the application of bamboo as structural materials, especially in densely populated spaces. To overcome the inherent deficiencies and use of bamboo in a safe manner, the antifungal and flame-retardant properties of bamboo needs attention.

In recent years, the photocatalytic semiconducting nanomaterials (such as TiO<sub>2</sub> [6–8], ZnO [9–12], CuO [13] and CeO<sub>2</sub> [14]) have been used in various applications in antibacterial and antifungal fields. However, the energy ranges of photoexcitation for many photocatalytic materials are relatively narrow. Furthermore, the photogenerated electron-hole pairs are easily recombined, which results in a low quantum efficiency. To improve the photocatalytic activity and take full advantage of solar light, the combination of nanomaterials with different band gaps has been considered as the most promising technology. It could effectively increase the separation efficiency of electron-hole pairs and extend the energy range of photoexcitation [15,16]. Therefore, the increased reactive oxygen species (ROS, such as •O<sub>2</sub><sup>-</sup>, •OH, and H<sub>2</sub>O<sub>2</sub>) would be produced.

Among the various photocatalytic nanomaterials, titanium dioxide (TiO<sub>2</sub>) and zinc oxide (ZnO) have received increasing attention because of their high chemical stability, nontoxicity, relatively low cost and high photocatalytic efficiency [17]. Several reports have demonstrated that ZnO-TiO<sub>2</sub> composites were quite effective when used as a photocatalyst [18–22], while the antifungal properties of bamboo modified with ZnO-TiO<sub>2</sub> nanocomposites have not been explored under solar light irradiation. Inspired by this, using the two nanomaterials to cover the bamboo substrate may improve the antifungal property in a natural environment and provide a flame-retardant property.

In this study, a facile method to synthesize the ZnO-TiO<sub>2</sub>-layered double-nanostructures on the bamboo substrate was proposed to modify the properties of bamboo in terms of the antifungal property, thermal stability and flame-retardant property. The morphology, crystallinity and chemical structure of the ZnO-TiO<sub>2</sub> coating were investigated. The ROS generated from ZnO-TiO<sub>2</sub> coating has been verified by electron spin resonance (ESR) tests under visible light irradiation. The mechanism of the improvement in its antifungal property has been proposed. Furthermore, the thermal stability and flame-retardant property were also evaluated.

## 2. Materials and Methods

### 2.1. Materials

Moso bamboo with a size of 50 mm (length) × 20 mm (width) × 6 mm (thickness) were first ultrasonically washed with deionized (DI) water and dried at 60 °C about 24 h before use. All the chemicals were of analytical reagent grade. The DI water was used throughout the experiment.

### 2.2. Synthesis of TiO<sub>2</sub> Thin Film on Bamboo Substrate

Firstly, a group of bamboo samples (12 pieces) was added to 400 mL of an aqueous solution containing 8.0 g of (NH<sub>4</sub>)<sub>2</sub>TiF<sub>6</sub> and 7.4 g of H<sub>3</sub>BO<sub>3</sub>. Using the liquid phase deposition method, the temperature of the solution was maintained at 80 °C for 5 h in a beaker. Subsequently, the samples were washed with DI water, before being dried at 60 °C for 24 h. The bamboo with a TiO<sub>2</sub> thin film were abbreviated as TiO<sub>2</sub>-B.

### 2.3. Synthesis of ZnO-TiO<sub>2</sub>-Layered Double-Nanostructures on Bamboo Substrate

Different concentrations of zinc nitrate solutions (0.05, 0.1, 0.2 and 0.3 M) were prepared to synthesize ZnO. The ammonia solution with a concentration of 28% was dropwise added to 400 mL of different concentration of zinc nitrate solutions under constant stirring until the solutions became clear. One group of TiO<sub>2</sub>-B was placed into the above mixture and heated at 80 °C for 3 h. Subsequently, the samples were washed with DI water, before being dried at 60 °C more than 24 h. The ZnO/TiO<sub>2</sub>-coated bamboo were abbreviated as ZnO/TiO<sub>2</sub>-B. For comparison, the pure ZnO coated bamboo samples were also prepared under the same conditions without the presence of TiO<sub>2</sub> and were abbreviated as ZnO-B.

#### 2.4. Characterization

The surface morphologies were observed by scanning electron microscopy (SEM, Hitachi SU8010, Tokyo, Japan) equipped with an energy-dispersive X-ray spectroscopy (EDS, OXFORD X-MAX80, Oxford, UK) system. The crystalline structures were identified by X-ray diffraction (XRD) using a Rigaku D/Max 2500 X-ray diffractometer (Rigaku, Tokyo, Japan) with Cu K $\alpha$  ( $\lambda = 1.5418 \text{ \AA}$ ) radiation at a scan speed of  $5^\circ \text{ min}^{-1}$  from  $10^\circ$  to  $80^\circ$ . The electron spin resonance (ESR) signals of the radicals trapped by 5,5-dimethyl-1-pyrroline *N*-oxide (DMPO) were obtained at room temperature with a Bruker (E580, Karlsruhe, Germany) spectrometer under visible light irradiation ( $\lambda > 420 \text{ nm}$ ). Thermogravimetric and Differential Thermal Analysis (TG-DTA) were measured by a NETZSCH TG-209F3 (Selb, Germany) thermogravimetric analyzer at a temperature of  $40\text{--}800^\circ\text{C}$  and a heating speed of  $10^\circ\text{C min}^{-1}$  under  $\text{N}_2$  atmosphere. The limiting oxygen index (LOI) was evaluated by a JF-5 oxygen index instrument (Nanjing Jiangning Company, Jiangning, China).

#### 2.5. Antifungal Test

The antifungal test was carried out in Hangzhou, China. Four groups of different samples (each group contains 12 pieces) were laid horizontally on a grid. The grid was 1 m above the ground and placed outdoors. Therefore, the samples were directly exposed to the natural environment. The temperature and weather during the test period were recorded. The antifungal test was performed from 24 April to 24 June 2018. It should be noted that the rainfall was sufficient in Hangzhou during this period, while the temperature and humidity were suitable for the growth of fungi. The antifungal properties of the samples were evaluated according to the Chinese Standard GB/T 18261-2013 [23]. The evaluation standards for the infection values are listed in Table 1.

**Table 1.** Rating scale for assessment of fungal growth.

Rating	Description
0	No fungal growth
1	The area of fungal infection is <25%
2	The area of fungal infection is 25%–50%
3	The area of fungal infection is 50%–75%
4	The area of fungal infection is >75%

### 3. Results and Discussion

#### 3.1. Morphological Observation

The microstructures of the pristine and functionalized bamboo were observed by SEM. It can be clearly seen that vascular bundles were embedded in the matrix of ground parenchyma from the SEM image of pristine bamboo (Figure 1a). After being coated with  $\text{TiO}_2$ ,  $\text{TiO}_2$  nanoparticles were uniformly distributed across the bamboo surface and formed a thin film (Figure 1b). The influence of the concentrations of ZnO nanostructures in the growth solutions were investigated, while other parameters remain unchanged (Figure 1c,d,f,g). Obviously, the content of the ZnO nanostructures on the  $\text{TiO}_2$  thin film increases with increasing ZnO concentration in the growth solution. At a relatively low concentration of 0.05 M, only a small amount of ZnO nanostructures formed and adhered to the  $\text{TiO}_2$  thin film. When the concentration increased to 0.1 M, the ZnO nanostructures were sufficiently continuous and uniformly distributed on the surface of  $\text{TiO}_2$  thin film. The cross-linked ZnO structures with an average thickness of approximately  $0.14 \mu\text{m}$  effectively improved the specific surface area of the ZnO- $\text{TiO}_2$  double-nanostructures coating. The average thickness of the ZnO- $\text{TiO}_2$  coating was approximately  $20 \mu\text{m}$  (Figure 1e). By contrast, the cross-linked structures disappeared when the growth solution concentration was at a high level ( $\geq 0.2 \text{ M}$ ), with the high-density ZnO nanostructures becoming a denser thin film and even covering the entire surface of bamboo.

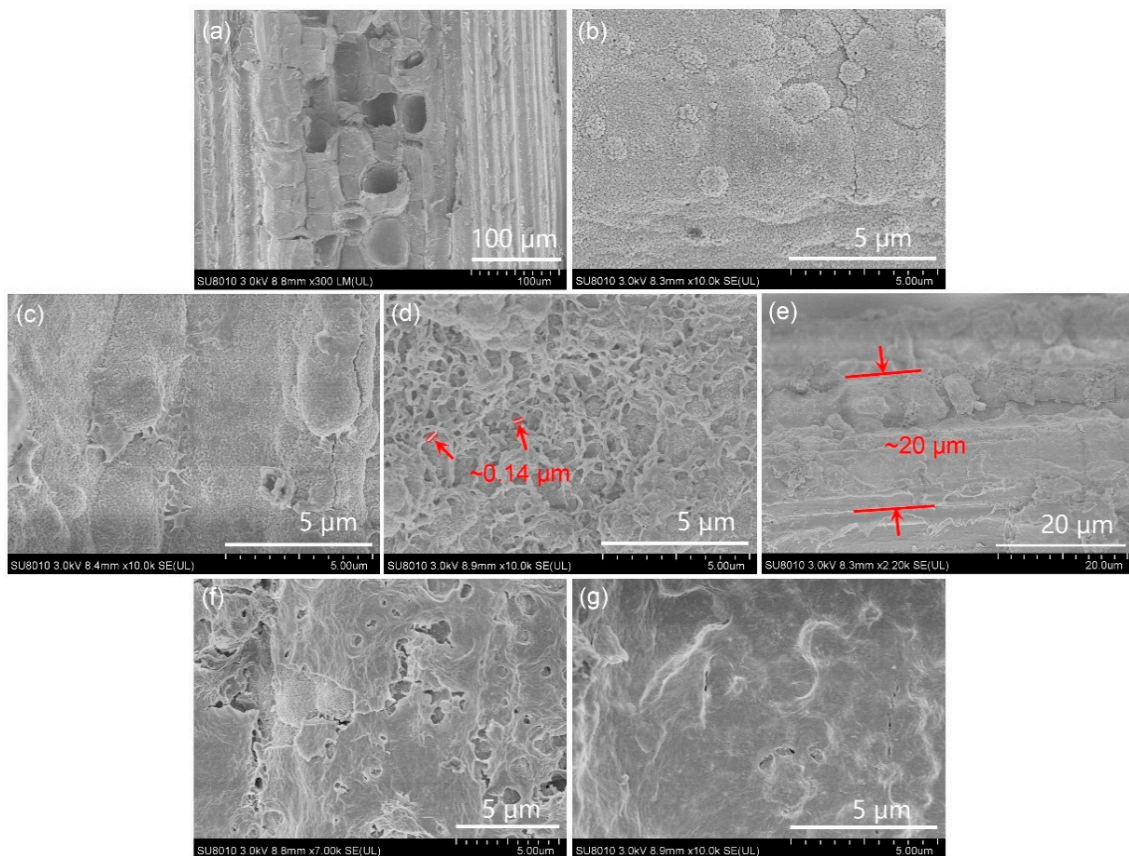
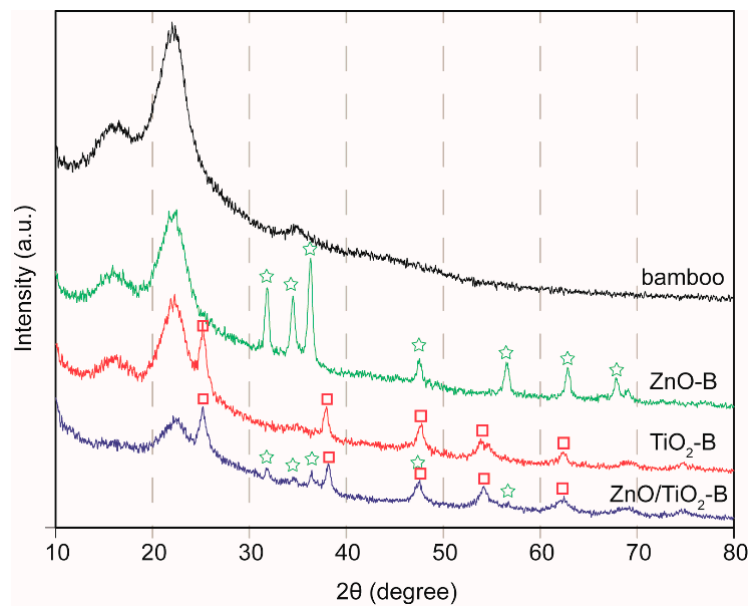


**Figure 1.** SEM images of (a) pristine bamboo; (b)  $\text{TiO}_2\text{-B}$  and  $\text{ZnO/TiO}_2\text{-B}$  with different concentrations of  $\text{Zn(NO}_3)_2$  during the coating process: (c) 0.05 M  $\text{ZnO/TiO}_2\text{-B}$ , (d) 0.1 M  $\text{ZnO/TiO}_2\text{-B}$ ; (e) The cross-section of the coating of 0.1 M  $\text{ZnO/TiO}_2\text{-B}$ ; (f) 0.2 M  $\text{ZnO/TiO}_2\text{-B}$ ; and (g) 0.3 M  $\text{ZnO/TiO}_2\text{-B}$ .

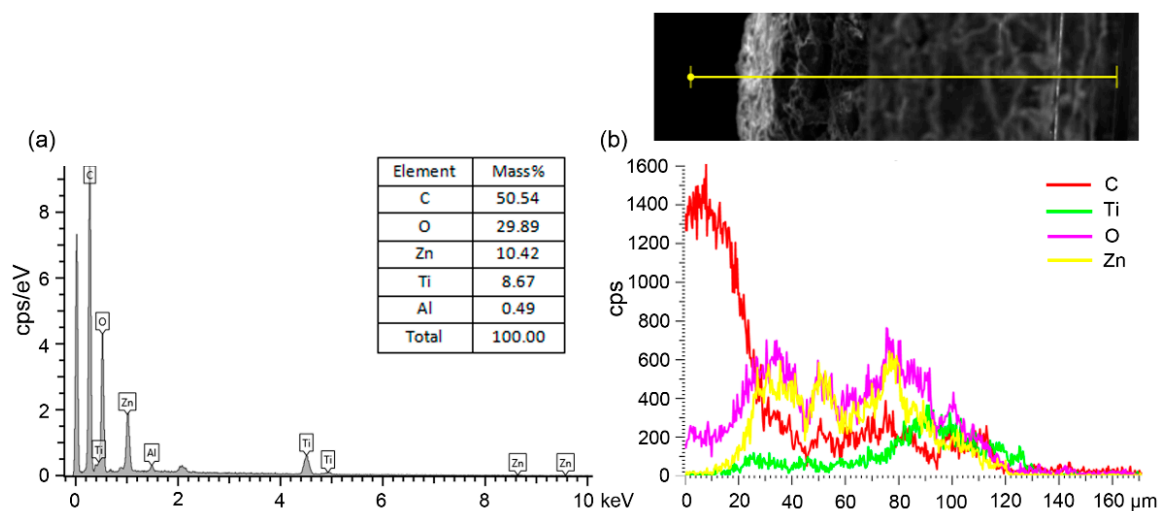
### 3.2. Elemental Composition and Crystalline Structure Analysis

Figure 2 presents the XRD patterns of pristine bamboo,  $\text{TiO}_2\text{-B}$ ,  $\text{ZnO-B}$  and  $\text{ZnO/TiO}_2\text{-B}$  (0.1 M of ZnO concentration in growth solutions). The peaks at  $16^\circ$  and  $22^\circ$ , which belong to the cellulose of bamboo, were detected in all the samples. The peaks assigned to the wurtzite ZnO (JCPDS cards: 36-1451) and anatase  $\text{TiO}_2$  (JCPDS cards: 21-1272) were respectively observed in  $\text{ZnO-B}$  and  $\text{TiO}_2\text{-B}$  [24,25]. Both peaks of ZnO and  $\text{TiO}_2$  appeared on  $\text{ZnO/TiO}_2\text{-B}$  and no other characteristic peaks were discovered. These observations demonstrated that the coating consisted of the wurtzite ZnO and anatase  $\text{TiO}_2$ . The EDS spectrum and SEM in the line scanning mode have provided evidence in the form of the above results and further confirmed the presence of the layered double nanostructures.

As shown in the EDS spectrum of the cross-section of  $\text{ZnO/TiO}_2\text{-B}$  (Figure 3), Ti, Zn, O, C and Al elements were observed. The element of C originated from the bamboo substrate or the conducting resin during SEM measurements, while the Al element could be expected from the sample stage. Figure 3b shows the relative intensity of each element measured along the coating (yellow line). The signal of oxygen (pink) implies that a large quantity of O element was distributed across the coating thickness. The signal of titanium (green) and the signal of zinc (yellow) indicated that the Ti and Zn elements were located on different layers of the  $\text{ZnO-TiO}_2$  coating, which revealed the layered double nanostructures. In short, the above analysis further confirmed that the  $\text{ZnO-TiO}_2$ -layered double-nanostructures were obtained and coated on the bamboo substrate.



**Figure 2.** XRD patterns of pristine bamboo, ZnO-B, TiO<sub>2</sub>-B and ZnO/TiO<sub>2</sub>-B.



**Figure 3.** (a) EDS spectra of the ZnO/TiO<sub>2</sub>-B and the content of each element (inset); and (b) SEM in the line scanning mode and the element distribution across the ZnO-TiO<sub>2</sub> coating.

### 3.3. Antifungal Property

Bamboo is easily degraded when directly exposed outdoors because of the organic nature of bamboo and the complex environmental conditions. The relevant research demonstrated that the optimum temperature for fungal growth is 5–30 °C, while the optimal humidity is above 63% [26]. The temperature and weather during the test period are presented in Figure 4a. As shown, the weather was mainly cloudy or rainy because of the upcoming rainy season in Hangzhou. The rainy season is very suitable for the growth of fungi. The results of the antifungal evaluation are summarized in Figure 4b. The photographs (front and back) of the samples after four weeks and eight weeks of the test are exhibited in Figure 5. Obviously, the pristine bamboo exhibited poor resistance to fungal growth, with fungi having grown after one week of being exposed outdoors. Furthermore, the infected area reached 100% after four weeks of the test. As shown in the photographs, the pristine bamboo surface was only severely degraded after four weeks of exposure. By contrast, ZnO-B and TiO<sub>2</sub>-B showed weak resistance to fungal growth. Fungi began to grow on ZnO-B during the third week and covered the entire surface after six weeks. For TiO<sub>2</sub>-B, there were significant differences between growth on the

front and the back as the fungi grew more easily on the back than on the front of the samples. After the two-month test, the face infection value of the front of TiO<sub>2</sub>-B was 43%, but the back reached 79%. The possible reason is that the back could not receive direct sunlight and the front of TiO<sub>2</sub>-B produced more ROS in the presence of light. As expected, ZnO/TiO<sub>2</sub>-B had an improved antifungal property as there were no visible fungi growth on both sides of the samples until the end of test.

To obtain more information of the fungal colonies, the samples were observed with an optical microscope after the two-month test period. As shown in Figure 6, fungi densely covered the entire surface of pristine bamboo. In contrast, the antifungal ability of TiO<sub>2</sub>-B was better than that of ZnO-B, and the ZnO-B was infected more severely. However, there was no visible fungal growth on the ZnO/TiO<sub>2</sub>-B surface, which indicated that ZnO-TiO<sub>2</sub> double-nanostructures coating effectively inhibited fungal growth on bamboo surface in an outdoor environment.

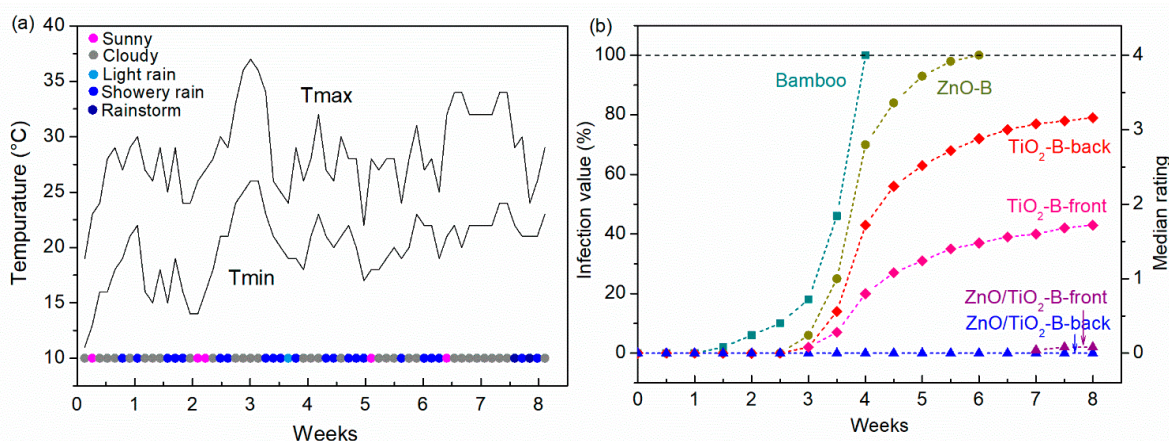


**Figure 4.** (a) The temperature and weather at test site from 24 April to 24 June; and (b) Median value of fungal growth on pristine bamboo, ZnO-B, TiO<sub>2</sub>-B and ZnO/TiO<sub>2</sub>-B.

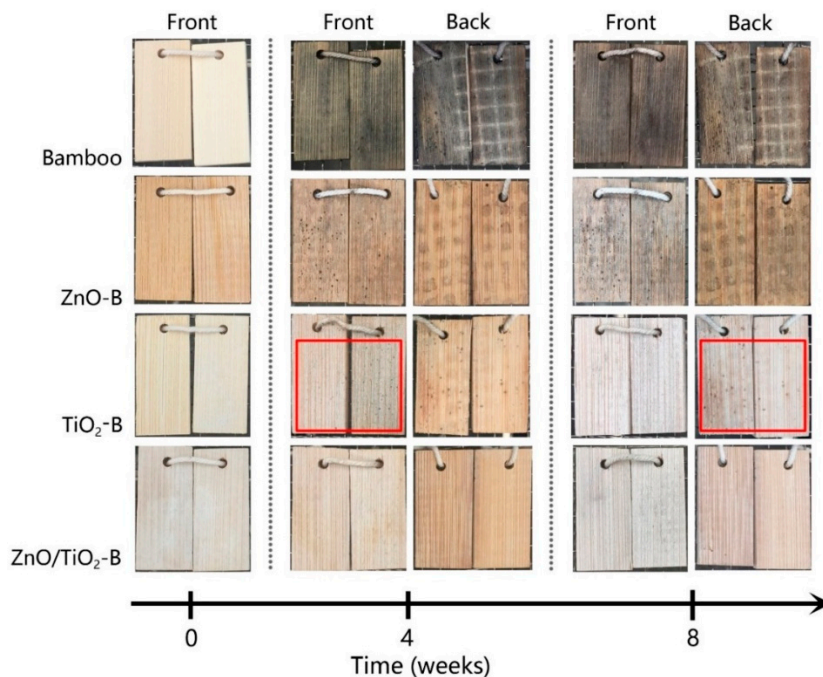


**Figure 5.** Digital photograph (front and back) of pristine bamboo, ZnO-B, TiO<sub>2</sub>-B and ZnO/TiO<sub>2</sub>-B after four weeks of exposure and eight weeks of exposure, respectively.

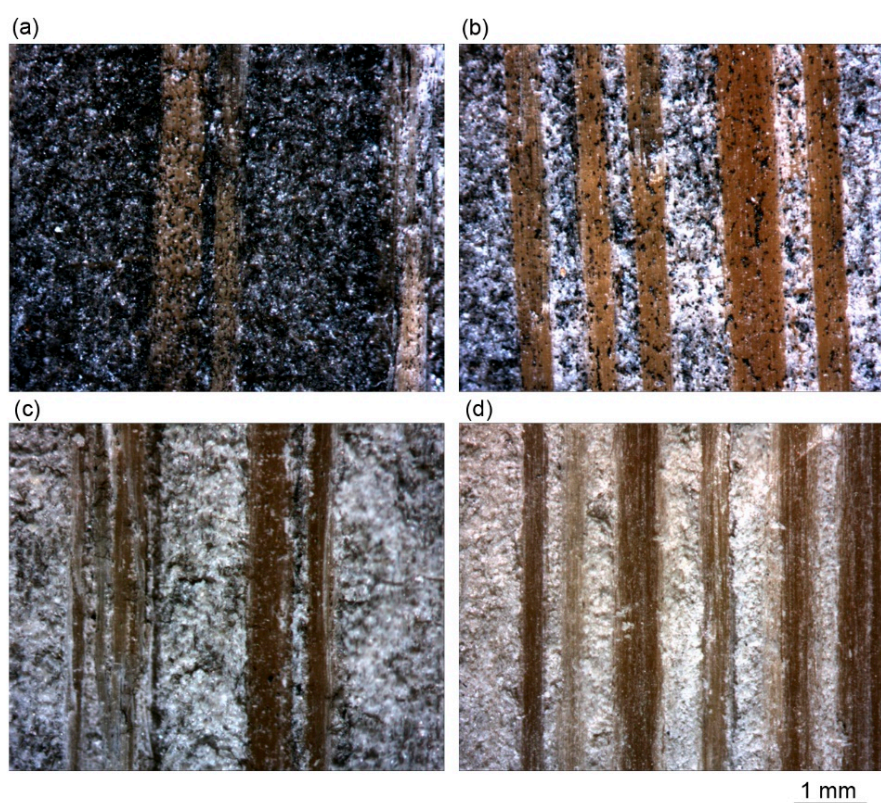


**Figure 6.** Optical microscope pictures after the two-month test period for (a) pristine bamboo; (b) ZnO-B; (c) TiO<sub>2</sub>-B; and (d) ZnO/TiO<sub>2</sub>-B, respectively.

### 3.4. Mechanism of the Enhanced Antifungal Properties

It is known that ROS have the ability to attack the crucial organic components of fungi and cause their death [27]. To identify the mechanism behind the improved antifungal property, the ESR spin-trap technique (with DMPO) was carried out to determine the photogenerated ROS from the surface of samples under visible light irradiation ( $\lambda > 420$  nm). The ESR spectra of DMPO- $\bullet\text{O}_2^-$  and DMPO- $\bullet\text{OH}$  are shown in Figure 7a,c. The characteristic peak with an intensity ratio of 1:2:2:1 were clearly observed. Due to the overall poor signal/noise ratio in certain samples, the quantitative analysis was performed by the highest signal/noise ratio in the 1:2:2:1 quartet profile, the quantified intensity of the second peak of the radical species (marked by the “\*”) are summarized in Figure 7b,d. Before the test, the characteristic signals intensity of the DMPO- $\bullet\text{O}_2^-$  for the samples were ZnO/TiO<sub>2</sub>-B > ZnO-B > TiO<sub>2</sub>-B. This revealed that ZnO/TiO<sub>2</sub>-B produced a greater amount of  $\bullet\text{O}_2^-$  than ZnO-B and TiO<sub>2</sub>-B under visible light irradiation [28–30]. There were no noticeable signals detected in pristine bamboo, which indicated that  $\bullet\text{O}_2^-$  could not be produced from pristine bamboo. For the ESR spectra of DMPO- $\bullet\text{OH}$ , under visible light irradiation, the characteristic signals intensity for ZnO/TiO<sub>2</sub>-B, ZnO-B and TiO<sub>2</sub>-B were basically the same. It demonstrated that this large quantity of  $\bullet\text{O}_2^-$  compared to  $\bullet\text{OH}$  is considered to be mainly responsible for the inactivation of fungi. Therefore, ZnO/TiO<sub>2</sub>-B had an improved antifungal property than ZnO-B and TiO<sub>2</sub>-B because more  $\bullet\text{O}_2^-$  was produced by ZnO/TiO<sub>2</sub>-B.

After the two-month antifungal test, the ROS signals of the samples were tested again. As shown, the intensity of ZnO/TiO<sub>2</sub>-B and ZnO-B for DMPO- $\bullet\text{O}_2^-$  was significantly reduced (Figure 7b). This might be due to the destruction of ZnO nanostructures by the rain wash in a natural environment, resulting in the gradual leaching of ZnO nanoparticles from the surface of the samples. As a consequence, the antifungal property of ZnO-B was weakened gradually. In contrast, the intensity of TiO<sub>2</sub>-B showed no significant decrease, which indicated that TiO<sub>2</sub> nanoparticles have a better resistance

leachability and it combined strongly with the bamboo substrate. Meanwhile, it is known that the band gap of  $\text{TiO}_2$  is narrower than that of  $\text{ZnO}$  and thus,  $\text{TiO}_2$  has a higher utilization rate of light. As a result, the antifungal activity of  $\text{TiO}_2$ -B was better than that of  $\text{ZnO}$ -B in an outdoor environment.

Based on the results of the antifungal properties of the samples and the characterization, the schematic of the mechanism behind the enhanced antifungal property for  $\text{ZnO}/\text{TiO}_2$ -B under solar light irradiation was proposed, which is shown in Figure 8 [18,31,32]. The  $\text{ZnO}$ - $\text{TiO}_2$ -layered double-nanostructures coating formed a heterojunction photocatalyst. Under solar light irradiation, the electrons were photoexcited from the valence band (VB) to the conduction band (CB) of  $\text{ZnO}$ , creating holes in the VB. After this, the photogenerated electrons ( $e^-$ ) in the CB of  $\text{ZnO}$  were transferred into CB of  $\text{TiO}_2$  because of potential difference between them, while the holes ( $h^+$ ) in the VB of  $\text{TiO}_2$  were transferred into the VB of  $\text{ZnO}$ . Simultaneously, because of the existence of electrons and holes, the dissolved molecular oxygen was reduced to  $\bullet\text{O}_2^-$  ( $\text{O}_2 + e^- \rightarrow \bullet\text{O}_2^-$ ) and the  $\text{H}_2\text{O}$  molecules were oxidized to  $\bullet\text{OH}$  ( $h^+ + \text{H}_2\text{O} \rightarrow \bullet\text{OH} + \text{H}^+$ ). Therefore, the electrons and holes were effectively separated and the generation of ROS was increased. According to the above analysis, the  $\text{ZnO}$ - $\text{TiO}_2$ -layered double-nanostructures improved the separation efficiency of electron-hole pairs, increased the generation of ROS and resulted in effective antifungal activity.

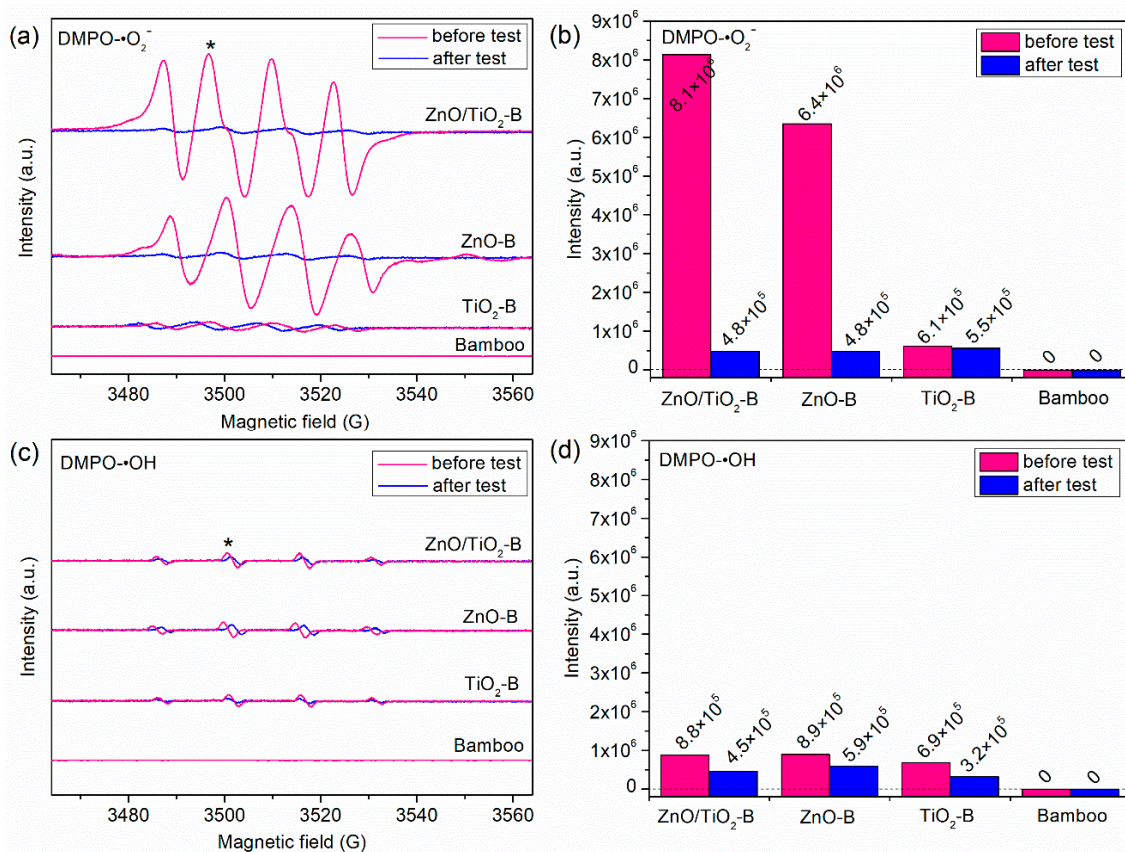


**Figure 7.** (a) The ESR spectra of  $\text{DMPO}\text{-}\bullet\text{O}_2^-$  before and after the two-month test; (b) the intensity of the second peak (marked by the “\*”) in the samples under visible light irradiation; (c) The ESR spectra of  $\text{DMPO}\text{-}\bullet\text{OH}$ ; and (d) the intensity of the second peak in the samples under visible light irradiation.

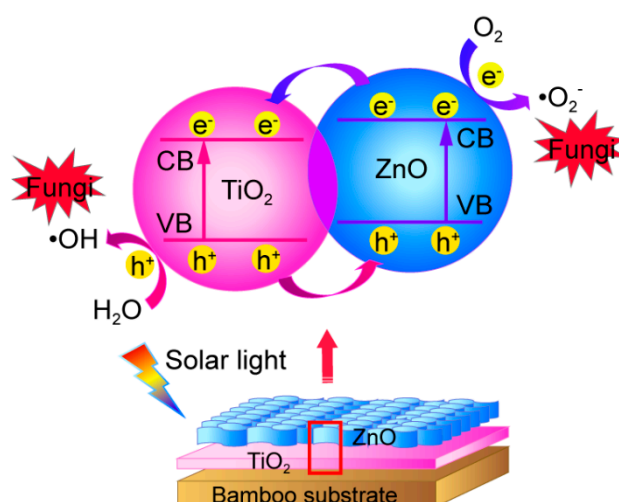


**Figure 8.** Schematic diagram of the enhanced antifungal property for the ZnO/TiO<sub>2</sub>-B under solar light irradiation.

### 3.5. Thermal Stability and Flame-Retardant Property

The TG and DTA curves of the samples are presented in Figure 9. As shown, the bamboo components were thermally degraded in three stages. The first decomposition process (190–250 °C) was assigned to the thermal depolymerization of hemicelluloses. The second decomposition process (250–380 °C) were ascribed to the cellulose decomposition and continuous degradation of lignin. During the third process (380–800 °C), the residual bamboo components continued to degrade, resulting in aromatization and carbonization [33–35]. After the calcining process, the weight of mass residues for pristine bamboo, ZnO-B, TiO<sub>2</sub>-B and ZnO/TiO<sub>2</sub>-B were 20.9%, 23.3%, 43.0% and 51.3%, respectively. In the DTA curve of the pristine bamboo, the two shoulder peaks located at 280 °C and 322 °C were assigned to the decomposition of hemicelluloses and cellulose, respectively. Compared to the pristine bamboo, the sharp endothermic peaks of ZnO-B, TiO<sub>2</sub>-B and ZnO/TiO<sub>2</sub>-B had a right-shift to 330, 345 and 337 °C, respectively. Meanwhile, the maximal pyrolysis rates were decreased. The maximal pyrolysis rate of ZnO/TiO<sub>2</sub>-B was decreased by 30.7%. This might be due to the decomposition of the ZnO-TiO<sub>2</sub> nanostructures coating, the strong interaction between ZnO and TiO<sub>2</sub> and the interaction between bamboo substrate and the coating. Comparing the four samples, ZnO/TiO<sub>2</sub>-B exhibited the lowest maximal pyrolysis rate and the highest weight of residues, which indicated that ZnO-TiO<sub>2</sub> nanostructures coating could act as a barrier and efficiently protect bamboo from the calcining process.

The flame retardancy property of the samples was determined by LOI, which is a common parameter used for assessing the flammability (Figure 9c). LOI refers to the minimum concentration of oxygen in an oxygen-nitrogen mixture [36]. It is determined as follows. A sample is ignited in an oxygen-nitrogen mixture. The oxygen concentration is adjusted until the minimum required to sustain steady burning is found. A higher LOI value indicates better flame-retardant capability. As shown, the pristine bamboo has a low LOI value of 25.6%. The LOI value of ZnO-B and TiO<sub>2</sub>-B increased to 27.8% and 28.3% because of the protective effects of ZnO and TiO<sub>2</sub> nanomaterials, respectively. After covering the bamboo substrate with ZnO-TiO<sub>2</sub> nanostructures, the LOI value increases dramatically to 30.2%, demonstrating the significant improvement in its flame-retardant property. Combined with the analysis of TG and DTA, ZnO-TiO<sub>2</sub>-layered double-nanostructures coating effectively improved the thermal stability and flame resistance of the samples, which provided a promising candidate for functional and building materials.

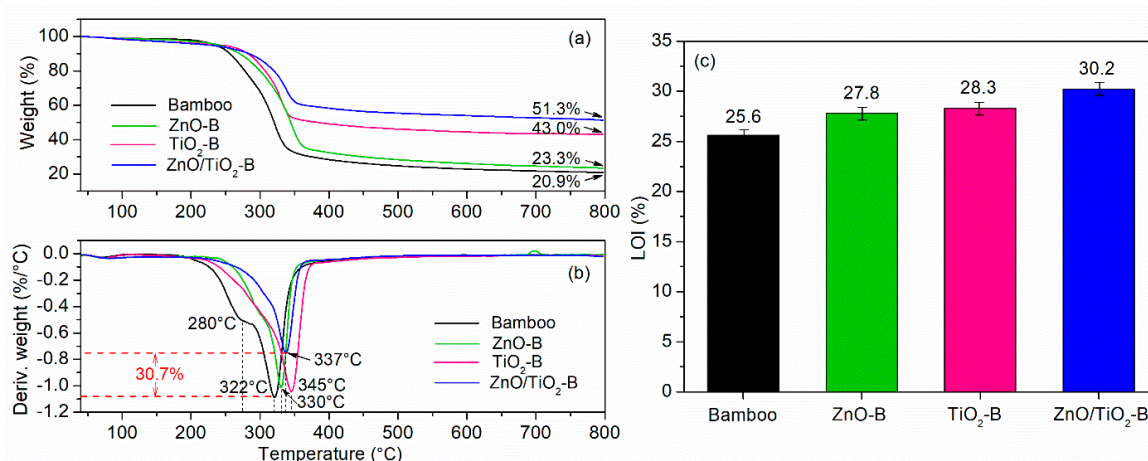


**Figure 9.** (a) TG curves; (b) DTA curves; and (c) LOIs of pristine bamboo, ZnO-B, TiO<sub>2</sub>-B and ZnO/TiO<sub>2</sub>-B.

#### 4. Conclusions

In this study, ZnO-TiO<sub>2</sub>-layered double-nanostructures were successfully coated on a bamboo substrate via a facile method to improve the antifungal and flame-retardant properties of bamboo. SEM, XRD and EDS confirmed that the ZnO-TiO<sub>2</sub> coating was a layered double nanostructure, which was successfully coated on the bamboo surface. During a two-month antifungal test in an outdoor environment, the ZnO-TiO<sub>2</sub>-layered double-nanostructures coated bamboo exhibited improved antifungal activity, which was due to the double nanostructures effectively increasing the separation efficiency of electron-hole pairs and extending the energy range of photoexcitation. ESR showed that the ROS of  $\bullet\text{O}_2^-$  and  $\bullet\text{OH}$  were generated on the ZnO-TiO<sub>2</sub> double-nanostructures surface under visible light irradiation ( $\lambda > 420$  nm). This large quantity of  $\bullet\text{O}_2^-$  compared to  $\bullet\text{OH}$  is considered to be mainly responsible for the inactivation of fungi. Furthermore, the ZnO-TiO<sub>2</sub>-layered double-nanostructures coating improved the thermal stability and flame-retardant property of bamboo, with the LOI value having increased to 30.2%. Therefore, we conclude that ZnO-TiO<sub>2</sub> double-nanostructures coating has a potential to inhibit fungal growth in an outdoor environment and to improve the flame-retardant property for protecting bamboo products.

**Author Contributions:** Conceptualization, J.L. and Y.C.; Formal Analysis, D.R. and J.X.; Investigation, D.R., Z.W., Y.B. and N.L.; Methodology, J.L.; Resources, Y.C.; Writing-Original Draft, D.R.

**Funding:** The research was funded by the Fundamental Research Funds for the Central Non-profit Research Institution of CAF (CAFYBB2017MA023), National Key Research and Development Program of China (2016YFD0600904) and Key Laboratory of High Efficient Processing of Bamboo of Zhejiang Province (2014F10047).

**Acknowledgments:** The authors wish to gratefully acknowledge the Zhejiang University for services related to SEM and EDS analysis of the samples.

**Conflicts of Interest:** The authors declare no conflicts of interest.

#### References

- Sharma, B.; Gatóo, A.; Bock, M.; Ramage, M. Engineered bamboo for structural applications. *Constr. Build. Mater.* **2015**, *81*, 66–73. [[CrossRef](#)]
- Verma, C.S.; Chariar, V.M. Development of layered laminate bamboo composite and their mechanical properties. *Compos. Part B Eng.* **2012**, *43*, 1063–1069. [[CrossRef](#)]
- Yu, Y.; Huang, X.; Yu, W. A novel process to improve yield and mechanical performance of bamboo fiber reinforced composite via mechanical treatments. *Compos. Part B Eng.* **2014**, *56*, 48–53. [[CrossRef](#)]
- Yu, Y.; Liu, R.; Huang, Y.; Meng, F.; Yu, W. Preparation, physical, mechanical, and interfacial morphological properties of engineered bamboo scrimber. *Constr. Build. Mater.* **2017**, *157*, 1032–1039. [[CrossRef](#)]

5. Flynn, A.; Chan, K.W.; Zhu, Z.H.; Yu, L. Sustainability, space and supply chains: The role of bamboo in Anji County, China. *J. Rural Stud.* **2017**, *49*, 128–139. [[CrossRef](#)]
6. Darbari, S.; Abdi, Y.; Haghighi, F.; Mohajezadeh, S.; Haghighi, N. Investigating the antifungal activity of TiO<sub>2</sub> nanoparticles deposited on branched carbon nanotube arrays. *J. Phys. D Appl. Phys.* **2011**, *44*, 245401–245410. [[CrossRef](#)]
7. Hou, X.; Ma, H.; Liu, F.; Deng, J.; Ai, Y.; Zhao, X.; Mao, D.; Li, D.; Liao, B. Synthesis of Ag ion-implanted TiO<sub>2</sub> thin films for antibacterial application and photocatalytic performance. *J. Hazard. Mater.* **2015**, *299*, 59–66. [[CrossRef](#)] [[PubMed](#)]
8. Akhavan, O. Lasting antibacterial activities of Ag-TiO<sub>2</sub>/Ag/a-TiO<sub>2</sub> nanocomposite thin film photocatalysts under solar light irradiation. *J. Colloid Interface Sci.* **2009**, *336*, 117–124. [[CrossRef](#)] [[PubMed](#)]
9. Chauhan, I.; Aggrawal, S.; Mohanty, P. ZnO nanowire-immobilized paper matrices for visible light-induced antibacterial activity against *Escherichia coli*. *Environ. Sci. Nano* **2015**, *2*, 273–279. [[CrossRef](#)]
10. Lipovsky, A.; Nitzan, Y.; Gedanken, A.; Lubart, R. Antifungal activity of ZnO nanoparticles—the role of ROS mediated cell injury. *Nanotechnology* **2011**, *22*, 105101–105105. [[CrossRef](#)] [[PubMed](#)]
11. Kairyte, K.; Kadys, A.; Luksiene, Z. Antibacterial and antifungal activity of photoactivated ZnO nanoparticles in suspension. *J. Photochem. Photobiol. B* **2013**, *128*, 78–84. [[CrossRef](#)] [[PubMed](#)]
12. Sharma, D.; Rajput, J.; Kaith, B.S.; Kaur, M.; Sharma, S. Synthesis of ZnO nanoparticles and study of their antibacterial and antifungal properties. *Thin Solid Films* **2010**, *519*, 1224–1229. [[CrossRef](#)]
13. Chen, X.; Ku, S.; Weibel, J.A.; Ximenes, E.; Liu, X.; Ladisch, M.R.; Garimella, S.V. Enhanced antimicrobial efficacy of bimetallic porous CuO microspheres decorated with Ag nanoparticles. *ACS Appl. Mater. Interfaces* **2017**, *9*, 39165–39173. [[CrossRef](#)] [[PubMed](#)]
14. Lu, Z.; Mao, C.; Meng, M.; Liu, S.; Tian, Y.; Yu, L.; Sun, B.; Li, C.M. Fabrication of CeO<sub>2</sub> nanoparticle-modified silk for UV protection and antibacterial applications. *J. Colloid Interface Sci.* **2014**, *435*, 8–14. [[CrossRef](#)] [[PubMed](#)]
15. Jing, L.; Xu, Y.; Huang, S.; Xie, M.; He, M.; Xu, H.; Li, H.; Zhang, Q. Novel magnetic CoFe<sub>2</sub>O<sub>4</sub>/Ag/Ag<sub>3</sub>VO<sub>4</sub> composites: Highly efficient visible light photocatalytic and antibacterial activity. *Appl. Catal. B Environ.* **2016**, *199*, 11–22. [[CrossRef](#)]
16. Xu, Y.; Liu, Q.; Liu, C.; Zhai, Y.; Xie, M.; Huang, L.; Xu, H.; Li, H.; Jing, J. Visible-light-driven Ag/AgBr/ZnFe<sub>2</sub>O<sub>4</sub> composites with excellent photocatalytic activity for *E. coli* disinfection and organic pollutant degradation. *J. Colloid Interface Sci.* **2018**, *512*, 555–566. [[CrossRef](#)] [[PubMed](#)]
17. Yin, Z.; Li, C.; Liu, X.; Feng, G.; Du, H.L.; Shi, L. Zn-doped TiO<sub>2</sub> nanoparticles with high photocatalytic activity synthesized by hydrogen–oxygen diffusion flame. *Appl. Catal. B Environ.* **2008**, *79*, 208–215. [[CrossRef](#)]
18. Lin, L.; Yang, Y.; Men, L.; Wang, X.; He, D.; Chai, Y.; Zhao, B.; Ghoshroy, S.; Tang, Q. A highly efficient TiO<sub>2</sub>@ZnO n-p-n heterojunction nanorod photocatalyst. *Nanoscale* **2012**, *5*, 588–593. [[CrossRef](#)] [[PubMed](#)]
19. Wang, Y.; Zheng, Y.Z.; Lu, S.; Tao, X.; Che, Y.; Chen, J.F. Visible-light-responsive TiO<sub>2</sub>-coated ZnO:I nanorod array films with enhanced photoelectrochemical and photocatalytic performance. *ACS Appl. Mater. Interfaces* **2015**, *7*, 6093–6101. [[CrossRef](#)] [[PubMed](#)]
20. Yuan, S.; Mu, J.; Mao, R.; Li, Y.; Zhang, Q.; Wang, H. All-nanoparticle self-assembly ZnO/TiO<sub>2</sub> heterojunction thin films with remarkably enhanced photoelectrochemical activity. *ACS Appl. Mater. Interfaces* **2014**, *6*, 5719–5725. [[CrossRef](#)] [[PubMed](#)]
21. Sun, W.; Meng, S.; Zhang, S.; Zheng, X.; Ye, X.; Fu, X.; Chen, S. Insight into the transfer mechanisms of photogenerated carriers for heterojunction photocatalysts with analogous positions of valence band and conduction band: A case study of ZnO/TiO<sub>2</sub>. *J. Phys. Chem. C* **2018**, *122*, 15409–15420. [[CrossRef](#)]
22. Cheng, P.; Wang, Y.; Xu, L.; Sun, P.; Su, Z.; Jin, F.; Liu, F.; Sun, Y.; Lu, G. High specific surface area urchin-like hierarchical ZnO-TiO<sub>2</sub> architectures: Hydrothermal synthesis and photocatalytic properties. *Mater. Lett.* **2016**, *175*, 52–55. [[CrossRef](#)]
23. GB/T 18261-2013 Test Method for Anti-Mildew Agents in Controlling Wood Mould and Stain Fungi; Standardization Administration of China: Beijing, China, 2013. (In Chinese)
24. Liu, B.; Sun, Y.; Wang, D.; Wang, L.; Zhang, L.; Zhang, X.; Lin, Y.; Xie, T. Construction of a branched ZnO-TiO<sub>2</sub> nanorod array heterostructure for enhancing the photovoltaic properties in quantum dot-sensitized solar cells. *RSC Adv.* **2014**, *4*, 32773–32780. [[CrossRef](#)]

25. Lachom, V.; Poolcharuansin, P.; Laokul, P. Preparation, characterizations and photocatalytic activity of a ZnO/TiO<sub>2</sub> nanocomposite. *Mater. Res. Express* **2017**, *4*, 035006. [[CrossRef](#)]
26. Li, J.; Yu, H.; Wu, Z.; Wang, J.; He, S.; Ji, J.; Li, N.; Bao, Y.; Huang, C.; Chen, Z. Room temperature synthesis of crystalline anatase TiO<sub>2</sub> on bamboo timber surface and their short-term antifungal capability under natural weather conditions. *Colloids Surf. A* **2016**, *508*, 117–123. [[CrossRef](#)]
27. Goffredo, G.B.; Citterio, B.; Biavasco, F.; Stazi, F.; Barcelli, S.; Munafò, P. Nanotechnology on wood: The effect of photocatalytic nanocoatings against *Aspergillus niger*. *J. Cult. Herit.* **2017**, *27*, 125–136. [[CrossRef](#)]
28. Velasco, L.F.; Carmona, R.J.; Matos, J.; Ania, C.O. Performance of activated carbons in consecutive phenol photooxidation cycles. *Carbon* **2014**, *73*, 206–215. [[CrossRef](#)]
29. Teng, W.; Li, X.; Zhao, Q.; Chen, G. Fabrication of Ag/Ag<sub>3</sub>PO<sub>4</sub>/TiO<sub>2</sub> heterostructure photoelectrodes for efficient decomposition of 2-chlorophenol under visible light irradiation. *J. Mater. Chem. A* **2013**, *1*, 9060–9068. [[CrossRef](#)]
30. Zhao, D.; Sheng, G.; Chen, C.; Wang, X. Enhanced photocatalytic degradation of methylene blue under visible irradiation on graphene@TiO<sub>2</sub> dyade structure. *Appl. Catal. B Environ.* **2012**, *111*, 303–308. [[CrossRef](#)]
31. Zheng, X.; Li, D.; Li, X.; Chen, J.; Cao, C.; Fang, J.; Wang, J.; He, Y.; Zheng, Y. Construction of ZnO/TiO<sub>2</sub> photonic crystal heterostructures for enhanced photocatalytic properties. *Appl. Catal. B Environ.* **2015**, *168–169*, 408–415. [[CrossRef](#)]
32. Xiao, F.X. Construction of highly ordered ZnO-TiO<sub>2</sub> nanotube arrays (ZnO/TNTs) heterostructure for photocatalytic application. *ACS Appl. Mater. Interfaces* **2012**, *4*, 7055–7063. [[CrossRef](#)] [[PubMed](#)]
33. Li, J.; Zheng, H.; Sun, Q.; Han, S.; Fan, B.; Yao, Q.; Yan, C.; Jin, C. Fabrication of superhydrophobic bamboo timber based on an anatase TiO<sub>2</sub> film for acid rain protection and flame retardancy. *RSC Adv.* **2015**, *5*, 62265–62272. [[CrossRef](#)]
34. Gao, L.; Lu, Y.; Li, J.; Sun, Q. Superhydrophobic conductive wood with oil repellency obtained by coating with silver nanoparticles modified by fluoroalkyl silane. *Holzforschung* **2016**, *70*, 63–68. [[CrossRef](#)]
35. Gao, L.; Lu, Y.; Zhan, X.; Li, J.; Sun, Q. A robust, anti-acid, and high-temperature–humidity-resistant superhydrophobic surface of wood based on a modified TiO<sub>2</sub> film by fluoroalkyl silane. *Surf. Coat. Technol.* **2015**, *262*, 33–39. [[CrossRef](#)]
36. Wang, J.; Jin, C.; Sun, Q.; Zhang, Q. Fabrication of nanocrystalline anatase TiO<sub>2</sub> in a graphene network as a bamboo coating material with enhanced photocatalytic activity and fire resistance. *J. Alloys Compd.* **2017**, *702*, 418–426. [[CrossRef](#)]



© 2018 by the authors. Licensee MDPI, Basel, Switzerland. This article is an open access article distributed under the terms and conditions of the Creative Commons Attribution (CC BY) license (<http://creativecommons.org/licenses/by/4.0/>).